Computational and Experimental Study of Stall Propagation in Axial Compressors

S. Jonnavithula,* S. Thangam,† and F. Sisto‡
Stevens Institute of Technology, Hoboken, New Jersey 07030

The paper presents a numerical and experimental study of stall propagation in axial compressors. In the numerical study, the compressor blades are represented as an isolated linear cascade of airfoils, and the stall propagation is simulated using a vortex tracking method. This method involves the use of periodic vortex arrays to simulate infinite cascades, the use of a vortex merging algorithm to allow computations for large times, the imposition of the no-slip and the impenetrability boundary conditions in an integral sense, the use of integral boundary-layer methods to locate the separation points, and the use of Fourier decomposition to compute the velocities of the propagating stall. Detailed parametric studies have been performed to analyze the influence of flows parameters such as the inflow angle and stall wavelength and geometric parameters such as cascade solidity, blade camber, and stagger. The experimental investigations were conducted in a single-stage axial compressor test rig. The occurrence of rotating stall in this research compressor was demonstrated, and some experimental studies on the effect of various flow parameters on the stall propagation were conducted. The computational and experimental results are compared and are shown to be in qualitative agreement.

Nomenclature

p = spatial period of the array
t = time
u,v = velocity components
V_p = velocity of stall propagation
V_t = tangential velocity (relative to the blade)
x,y = Cartesian coordinates
z = complex variable, $z = x + iy$
α = inflow angle
Γ = circulation
γ = stagger angle
θ = camber angle
σ = bounded support for vortex blobs
ψ = stream function
ω = vorticity

I. Introduction

IT is well known that when the volume flow rate through an axial flow compressor is reduced steadily by throttling, the compressor begins to stall at a critical value of the flow coefficient. Under certain flow conditions, the flow does not stall uniformly on all blades. Instead, one or more groups of blades stall, and this stalled region "propagates" in the direction of the rotation of the compressor but with a lower velocity. This propagating stall, also called rotating stall, is quite undesirable because of the cyclic loadings on the blades, which can cause aeroelastic vibration and fatigue failure.[1,2]

Because of the obvious complexities of the flow in a stalled compressor, most theoretical studies of this phenomenon have necessarily been confined to simplified "actuator disk" representations.[3] Traditional numerical methods such as the finite-difference method are not very well adapted to the study of this type of flow because of the high Reynolds numbers involved and the complex flow geometries. The vortex method, on the other hand, is ideally suited to provide a natural and efficient description of the shed eddies. A significant advantage of this method is that in the large irrotational regions, no vortices are needed, and thus the computational domain extends effectively to infinity. Earlier versions[4] of the vortex method modeled the flow downstream of the cascade as a sequence of Karman vortex streets consisting of one street for each stall cell. The strength of each vortex was either positive, representing the shed lifting vortex, or negative, representing the corresponding starting vortex occasioned by lift recovery. Stemming from the simplifying assumptions employed in the model, only velocity of propagation could be computed; neither the cell width nor stability considerations could be developed. The present vortex model nevertheless may be considered as a refinement of the earlier vortex method with additional important features made possible by the increase in computational speed and storage of the present generation computers.

It should be noted here that while in practical applications the flowfield in a turbomachine is three dimensional,[5] the present work concerning the flowfield in a linear cascade analyzes only the two-dimensional subset of this very complicated problem. Thus, the conclusions and implications derived from this study are expected to be qualitatively correct. However, this limitation is not ultimately debilitating since the radial components of velocity are thought to be symptomatic, summoned into being by the low through-flow components within the stall cells and not the cause, so-to-speak, of the appearance of propagating stall cells. (This should of course not be taken to minimize the potential and importance of three-dimensional effects.)

There is a fundamental difference, therefore, between the stall of a cascade of blades and a single airfoil; the blades that are stalled, and therefore within the stall cells, temporarily inhibit the stall of the other blades outside the cells. Thus, although the effect on parameters such as pressure ratio and deflection integrated over the flow annulus may very smoothly as the mean incidence is increased, the local unsteady flows

Received May 16, 1989; presented as Paper 89-2454 at the AIAA/ASME/ASEE/SAE 25th Joint Propulsion Conference, Monterey, CA, July 10–12, 1989; revision received and accepted for publication Nov. 20, 1989.

*Engineer; currently at Analysis and Design Applications Co.
†Associate Professor. Member AIAA.
‡George Meade Bond Professor. Associate Fellow AIAA.

about a particular blade vary quite dramatically as the blade is first enveloped and then cleared by a stall cell. This local behavior explains the random, or chaotic, content of the velocities and pressures; in nonlinear systems there is a sensitive dependence of behavior on initial conditions. This chaotic, or random, content usually constitutes a noise level with a broad frequency spectrum. The overall propagating stall phenomenon is still deterministic but is not amenable to small perturbation analysis, which applies principally to linear systems.

This study shows that the imposed periodicity constrains the occurrence of stable propagating stall to a limited range of flow and geometric parameters. It is found that within this stable range, the vortex method is quite robust and insensitive to the influence of nonphysical parameters. A systematic parametric study is conducted within the stable ranges to extend the available results. The parametric study analyzes the influence of cascade parameters such as the inflow angle, imposed wavelength, blade camber, cascade solidity, and stagger angle on the stall propagation. A brief description of experiments conducted in the single-stage axial compressor test rig is also provided along with a comparison of the experimental and computational results.

II. Computational Model and Method of Solution

The flow configuration being studied here is illustrated in Fig. 1. A reference frame fixed to the cascade is used. Thus, the blades are at rest and the stall cell moves past them. The y axis represents the tangential direction and the x axis, the axial direction. The inflow angle α is measured with respect to the axial direction in this frame. The stagger angle γ and the camber angel θ are marked on the sketch.

The physical configuration consists of a linear cascade of staggered, cambered airfoils in high Reynolds number two-dimensional flow. As in physical applications involving axial-flow turbomachinery, these blades are subject to self-excitation. A vortex method first proposed by Spalart[6] for a stationary cascade was later successfully modified and refined for the analysis of stall propagation by Jonnavithula.[7] In the following, a brief description of the formulation and the method of solution will be given.

For two-dimensional, viscous, incompressible flow past an infinite linear cascade of airfoils at high Reynolds number, the basic aerodynamic equations that govern the vorticity field are as follows.

$$(\partial_t + u\partial_x + v\partial_y)\omega = 0 \tag{1}$$

where

$$\omega = \partial_x v - \partial_y u \tag{2}$$

A stream function ψ can be defined to satisfy the continuity equation such that

$$u = -\partial_y \psi \quad \text{and} \quad v = \partial_x \psi \tag{3}$$

Combining Eqs. (2) and (3),

$$\nabla^2 \psi = \omega \tag{4}$$

The vortex method involves the discretization of the computational domain into a large number of finite vortex blobs that convect with the mean flow but do not change their strength; i.e.,

$$\omega = \sum_{k=1}^{N} \omega_k \tag{5}$$

The corresponding stream function induced by the collection of vortices ψ_k is readily determined[8]

$$\psi_k = \frac{\Gamma_k}{4\pi} \ell n \left\{ \left| \sin\left[\frac{2\pi i}{P} (z - z_k) \right] \right|^2 + \sigma^2 \right\} \tag{6}$$

Here, Γ_k is the circulation of the kth vortex blob, $i \equiv \sqrt{-1}$, the complex variable $z = x + iy$, and p is the period of the array. The parameter σ smooths out the singularity at $z = z_k$.

The vortex tracing algorithm used in this study has been described earlier.[6,7] Briefly, the no-slip boundary condition and the impenetrability boundary condition are imposed in an integral sense by the creation of a discrete vortex sheet about each airfoil at each time step. An integral boundary-layer routine is used to compute the separation point on each airfoil, and only vortices created downstream of separation point are allowed to convect; the rest are considered "bound vortices" and reabsorbed at the next time step. These "free" vortices are tracked using a second-order integration of the induced velocity at their centers. A merging algorithm is used to keep the number of vortices approximately constant in spite of creating new vortices at the boundaries at each time step. To simulate an infinite cascade of airfoils, the periodicity assumption is made in the tangential direction. That is, a vortex leaving the top of the computational domain is assumed to reappear at the bottom. The number of airfoils in each period is specified in advance, and each vortex in the domain is assumed to represent one of an infinite array of vortices lying outside the fundamental period. The entire time-marching computation begins with an initial disturbance of two countervortices placed in the flowfield and subsequently convected out of the computational domain.

The results of the computation are the vortex strengths and positions at each time step. The resultant velocity field including the vortex-induced components can be computed from these for display purposes, although it is not needed for the computation of stall propagation. The propagation velocity is computed as follows. The axial velocity is computed at a number of points equally spaced along the tangential direction at one particular axial location. The phase of the first (spatial) Fourier component of these velocities is used to find the position of the stall (the minimum velocity region). The velocity of propagation is then computed as the time rate of change of position. Typical results of this procedure are shown in Figs. 2 and 3. Figure 2 shows the streamlines of the flow in a particular configuration at equally spaced instants of time. Note that two periods are plotted in the tangential direction to show clearly the passing of the stall cell from the top of the period to the bottom of the next period. It can be

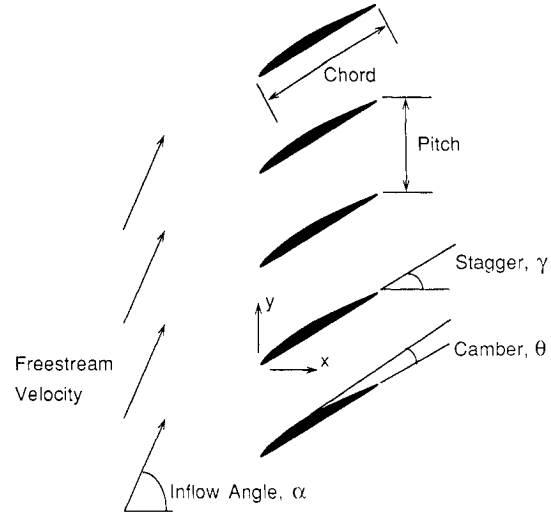

Fig. 1. Schematic of the flow configuration.

seen that there is a region of stalled flow that propagates tangential (upward in the figure). A qualitative assessment of the magnitude of the flow perturbations may be obtained by an examination of these streamline plots.

Figure 3 shows the position of the stall from the Fourier analysis. After a short initial transient, the points fall very closely on a straight line. The slope of this line (obtained through a least-square analysis) then gives the velocity of propagation. The plot of the position of the phase of the Fourier component, referred to as the phase plot, can be seen to be much more informative than the streamline plots and is used exclusively in the rest of this report for comparisons. One important point that should be made about this plot is that the actual values of the position are irrelevant. Only the slope of the curve, which gives the velocity, is of significance in making comparisons.

One of the basic differences between the present vortex method and earlier versions is the vortex merging algorithm. The use of a vortex merging scheme makes it possible to satisfy the zero velocity boundary conditions at the solid boundaries with a high resolution at each time step by releasing many new vortices, and still limits the total number of vortices in the computational domain to a manageable number by merging vortices (i.e., making the discretization coarser) further from the body. A detailed description of the merging algorithms analyzed may be found elsewhere.[7,9]

In addition to the influence of the merging strategy, the effects of other program parameters such as the time step and the number of vortices were exhaustively investigated. It was found that for combinations of flow parameters that lead to stably propagating stall, these parameters could be varied over a wide range without affecting the computed values of the stall propagation velocities.

All computations reported in this work were performed using a Cray X-MP/48 supercomputer. Fifty boundary points were used to define each solid body, and the number of vortices in the flowfield was kept at six times the total number of boundary points. Thus, for a three-blade cascade, 900 vortices were used. A typical computation involved time marching over 2000 steps (of size 0.05 time units) and required approximately 20 min of CPU time for a three-blade cascade. This large amount of computational time is closely related to the number of vortices and the number of time steps, since at each time step the effect on each vortex of every other vortex in the computational domain must be computed.

III. Computational Investigations

An earlier work[10] presented the preliminary results of a parametric analysis of propagating stall. Among the parameters considered were the inflow angle, the cascade stagger, blade camber, and the imposed disturbance wavelength. It was found that the stagger angle, the inflow angle, and the blade camber each had a strong effect on the velocity of propagation; while the imposed wavelength had only a minor effect. On this basis, it was concluded that the choice of the imposed wavelength did not significantly affect the wave celerity and was to a certain extent an arbitrary parameter.

In attempting to generate results for a wider range of parameters, however, it was found that the computed values of propagation velocity fluctuated widely with small changes in flow parameters over certain ranges of these parameters. The reason was that, over these ranges, the natural wavelength of the propagating stall was different from the computationally imposed wavelength. In a real compressor, the number of stall cells and hence the width of each cell would automatically adjust themselves to the flow conditions. As the flow is throttled, propagating stall usually begins with a large number of stall cells of small circumferential extent. Further throttling has the effect of collapsing these cells into larger ones, until at the surge limit, there is one large cell covering almost half the circumference of the compressor. In the computation, on the other hand, a fixed stall wavelength (circumferential extent) is selected independently of the flow conditions and thus cannot be expected to be correct at all flow angles. A detailed discussion of this aspect is given in Sec. V and in Jonnavithula.[7]

The above point about stable regions helps set in perspective the parametric studies described below. For an assumed stall cell wavelength, only some flow conditions yield stall. Keeping these restrictions on allowable ranges of the parameters in mind, a comprehensive parametric study is then attempted for the parameters of greatest practical interest, namely, the inflow angle α, the stagger angle γ of the cascade, the blade camber, and the cascade solidity. For each configuration, multiple runs were conducted with slightly different time steps to establish that there was indeed a stable propagating stall. In all the subsequent figures, only the stable regions as identified by this procedure are presented. A line is fitted to the period data by a least-squares procedure so that comparison of trends becomes possible. The results presented in this section analyze the influence on the velocity of stall propagation of cascade parameters such as the blade camber, the cascade solidity, and the cascade stagger.

Figure 4 shows the effect of the blade camber on the velocity of propagation for a three-blade cascade set at zero stagger with an inflow angle of 55 deg. The different cambered blades were obtained by mapping the NACA0008 thickness distribution onto circular arc mean camber lines. The results

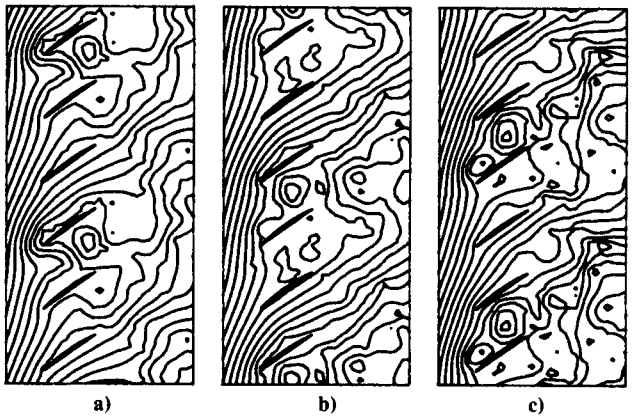

Fig. 2 Streamlines for stall propagation in a three-blade cascade (two identical periods are shown; in each case stagger = 35 deg, camber = 10 deg, inflow angle = 75 deg); time levels are a) $t = 42$; b) $t = 46$; c) $t = 50$.

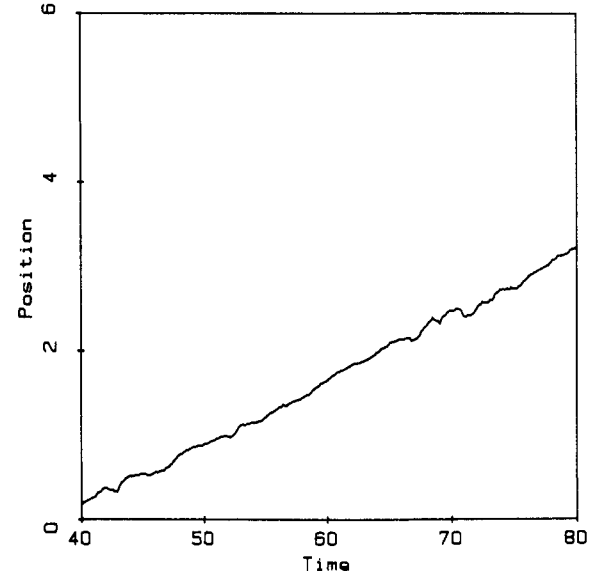

Fig. 3 Position of stall cell vs time for the flowfield shown in Fig. 2.

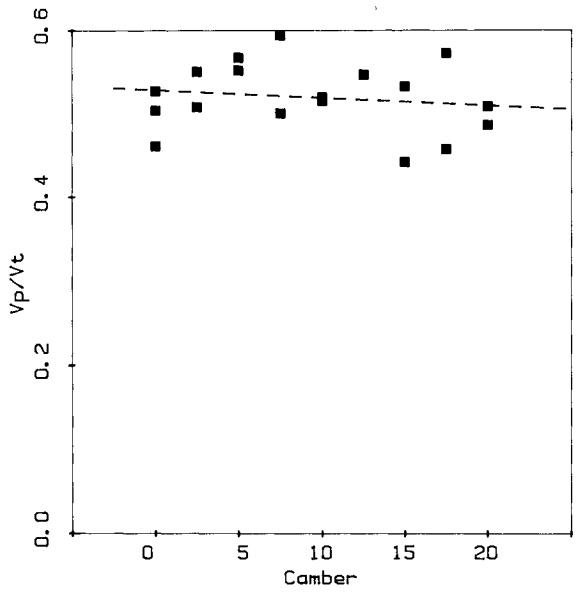

Fig. 4 Influence of blade camber on the normalized stall propagation velocity in a three-blade cascade (stagger = 0 deg, inflow angle = 55 deg, solidity = 1).

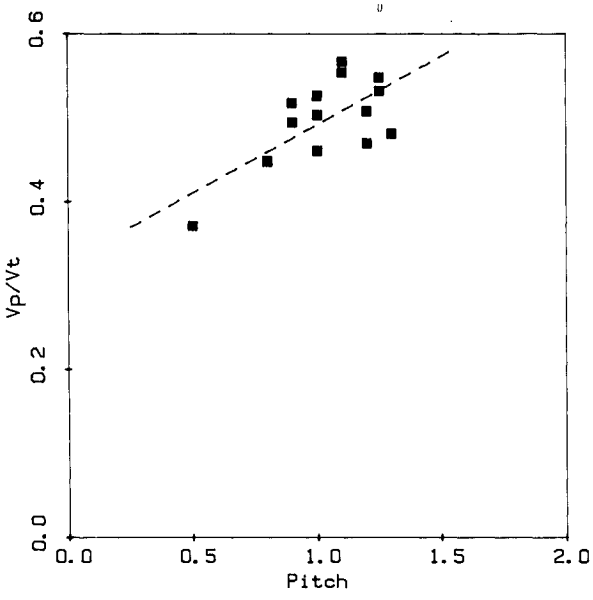

Fig. 5 Influence of blade pitch on the normalized stall propagation velocity in a three-blade cascade (camber = 0 deg, stagger = 0 deg, inflow angle = 55 deg).

show a considerable scatter, but it is clear that there is no consistent trend in the data. The least-squares fit confirms this showing a very small change in velocity with camber.

The physical explanation for the lack of influence of the camber is that at the high flow angles used, the flow was separated and hence was not influenced by the relatively small changes in the shape of the airfoil. On physical grounds, it may be expected that highly cambered blades would begin to stall at lower incidence angles. This was confirmed numerically with a three-blade cascade of 20-deg camber, which exhibited propagating stall at incidence angles as low as 40 deg. Additional discussions on this aspect of the parametric study is given in Jonnavithula.[7]

Figure 5 shows the effect of blade pitch in a three-blade cascade at zero stagger with the inflow angle of 55 deg. The velocity of propagation is a strong function of pitch, increasing rapidly with it. A physical reason for this effect may be suggested by examining the process by which the stall propagates. For the stall to propagate, the flow conditions at the stalled blade must influence the conditions at the next blade. The time taken for these disturbances to travel depends primarily on the chordwise inertia of the fluid; the boundary-layer time lag is relatively independent of the pitch. The propagation velocity for given flow conditions (which is defined as the pitch divided by the total time taken to travel from one blade to the next), therefore, increases with an increase in pitch.

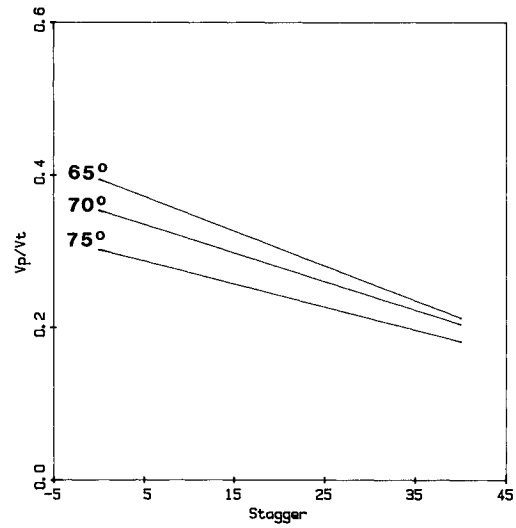

Fig. 6 Influence of blade stagger on the normalized stall propagation velocity in two-blade cascades of 10-deg camber at inflow angles of 65, 70 and 75 deg.

Figure 6 shows the variation of the normalized velocity of propagation for three different inflow angles in a two-blade cascade for stagger angles ranging from 0 to 45 deg. As can be seen, the velocity of propagation decreases with increasing stagger angles for the three inflow angles considered. However, the variation of stall propagation velocity with blade stagger is quite complex and depends not only on the inflow angle but also on parameters such as the number of blade passages. A detailed discussion of the effect of stagger angle and imposed period may be found elsewhere.[7,9]

IV. Experimental Study

The validity of two-dimensional cascade computations for the prediction of propagating stall in the flow annulus of an axial compressor has often been called into question. Clearly, when stall cells appear in a real compressor, the low-velocity regions within the stall cells and the higher through-flow components outside the cells are both subjected to the same radial and axial pressure gradients. The demands of radial equilibrium therefore suggest that appreciable radial components of velocity develop within the cells, and an extremely complex overall flow pattern emerges. The full Navier-Stokes equations, expressed in both relative and absolute coordinates, govern the evolution of the actual highly unsteady flowfield. With this understanding, one would expect the compressor flow to approach two-dimensional cascade flow for high hub/tip ratios and low-amplitude stall. The experiments on the Stevens single-stage research compressor attempted to assess the limiting behavior subject to the pre-existing geometry of the compressor.

The experiments reported herein are more fully described elsewhere.[7] The single-stage research compressor has a tip diameter of 0.5 m (20 in.) and a hub/tip ratio of 0.6. The 36 rotor blades were untwisted and untapered with a camber of 10 deg, a chord of 5 cm (2 in.) and a thickness of 4.3%. The rotor stagger is 45 deg, and a row of 29 twisted inlet guide vanes (IGVs) is located $4\frac{1}{2}$ chords upstream of the rotor

(center-to-center); the setting can be varied from +10 to −20 deg at the mean radius. There are no downstream stators in the compressor.

The principal instrumentation consists of three hot-wire/hot-film anemometer probes inserted at three circumferential locations upstream of the rotor. These probes were set at unequal angular separations to resolve the ambiguity in the actual number of stall patches occurring in the flow annulus. One probe, with a crossed wire sensing element, was capable of conducting radial transfer from midradius to ±31% of the annulus height. Further details concerning instrumentations, calibrations, ancillary equipment, data recording, and reduction appear in Jonnavithula.[7]

The two principal measurements of interest were the number of stall cells and the stall propagation rate. In addition, radial survey of the velocity gave a qualitative measure of the intensity and distribution of the stall disturbance. These data augmented the information obtained from the probe set at midradius and from which a continuous record of the velocity was obtained. Figure 7 shows a sequence of records for a series of decreasing flow coefficients at constant rotor speed.

Figure 8 displays the axial, tangential, and total velocity as well as the flow angle at six different radial positions during the passage of one stall cell. Propagation rates were obtained by effectively counting the number of peaks on the voltage traces in a known interval of time after resolving the number of cells present. In practice, the peak counting was performed using a real-time spectrum analyzer processing the signal from the hotwire probe.

V. Analysis of Computational and Experimental Results

Of greatest interest was the comparison of the computed propagation rate with the experimental value from the compressor measurements. For this purpose the blade geometry, speed, and mean flow conditions of the test compressor at mean radius were inputs to the vortex method predictions of the propagation rate assuming two-dimensional flow. The results of these calculations and comparisons appear in Fig. 9. Therein it is noted that the computed results depend critically upon the presumption of the integral number of blade passages corresponding to the stall-cell wavelength. The computations are based upon assuming 2, 3, or 4 passages for the wavelength parameter.

It is seen that the normalized propagation velocity agrees qualitatively as to magnitude and trend with a cascade of 12 pitch wavelength, the figure corresponding to the experiments in the compressor (36 rotor blades with 3 stall patches). It was unfortunate that the need to make a series of computer runs with 12-blade periodicity was not identified until late in the program. The computer runs would have been extremely extensive since the computing time of the present algorithm varies geometrically with the number of passages in the period.

It should be noted that the question of stability with respect to the stall propagation rate has a number of important aspects, both computational and physical. As indicated earlier, the periodicity condition in which a small integral number of blades in the cascade were defined as one period was used to simulate an infinite cascade, and the flow phenomena

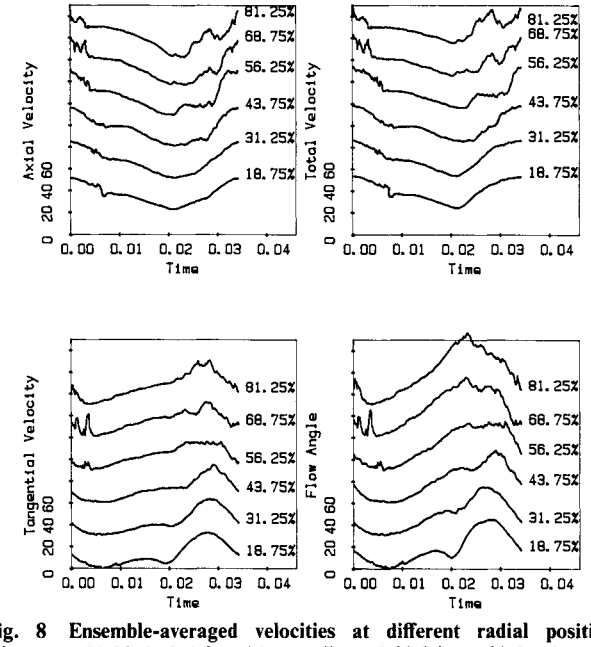

Fig. 8 Ensemble-averaged velocities at different radial positions (shown as % blade height with an offset of 30 ft/s or 30 deg between successive curves).

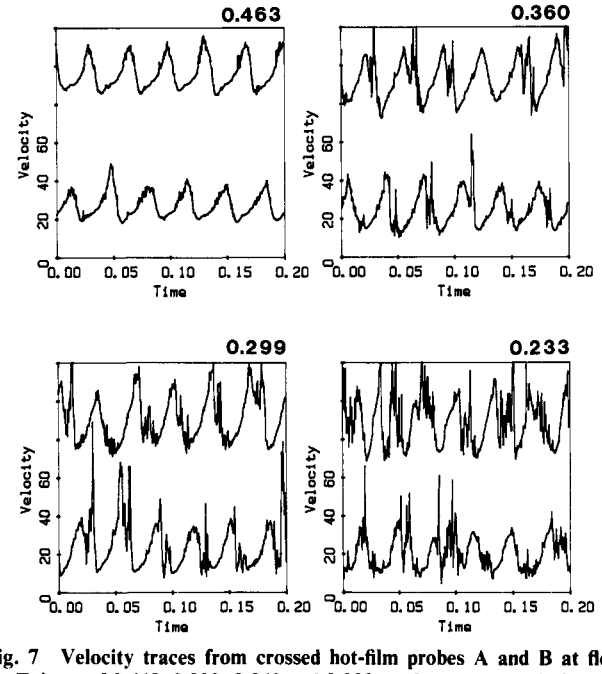

Fig. 7 Velocity traces from crossed hot-film probes A and B at flow coefficients of 0.463, 0.299, 0.360 and 0.233; each upper trace is for film A, and each lower trace is for film B; an offset of 60 ft/s has been added to each upper trace.

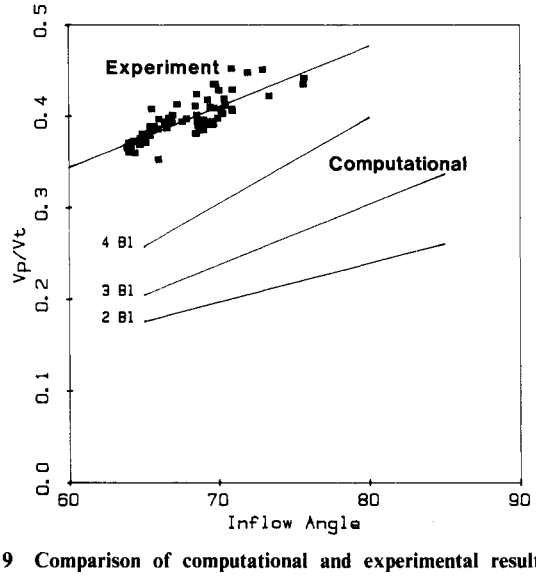

Fig. 9 Comparison of computational and experimental results; the lower curves are computational results for two-, three-, and four-blade cascades, and the upper plot is the experimental data (with a wavelength of 12 blades).

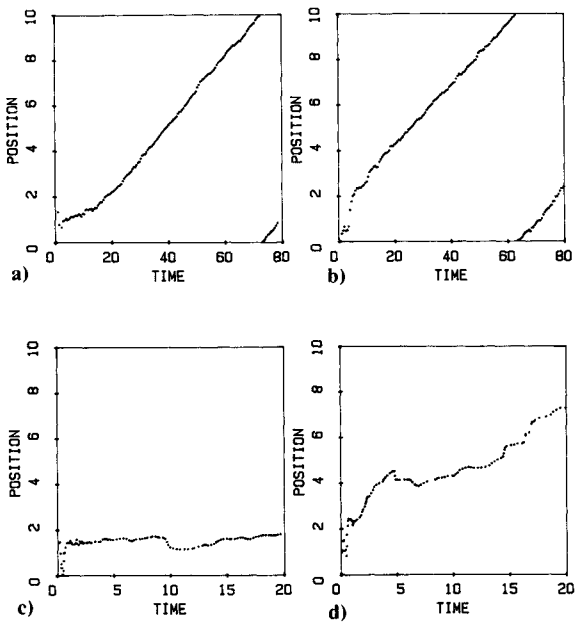

Fig. 10 Effect of small change in time step for stable stall propagation; plots a) and b) are for a two-blade cascade with stagger = 10 deg, inflow angle = 76 deg and time steps 0.049 and 0.05; c) and d) are for the same cascade at an inflow angle = 63 deg with the same time steps.

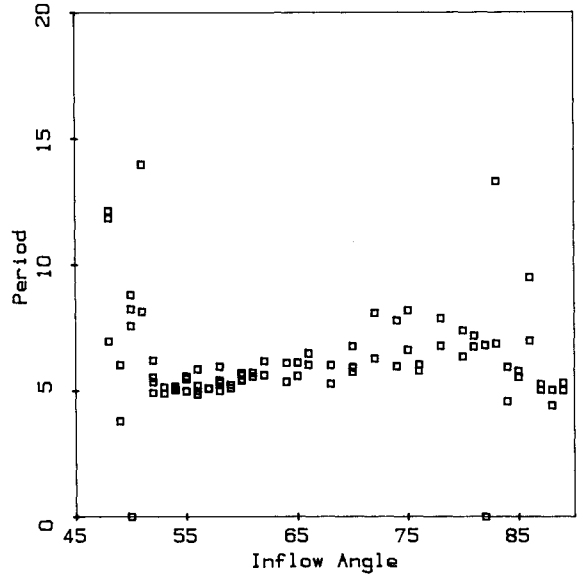

Fig. 11 Variation of stall propagation period with inflow angle in a two-blade cascade at 0-deg stager; time steps of 0.048, 0.049, 0.050, and 0.051 are used to obtain the values (stable region is from 53 to 70 deg).

were assumed to be identical in all periods. The largest period used consisted of six blades, although typical periods were two, three, and four. The upper limit is set by computer limitations, as the time and memory requirements increase rapidly with the number of blades retained in each period.

In a real compressor, the stall-cell width is determined by the flow conditions. Typically, rotating stall starts with a large number of small cells as the flow is throttled, the number of cells decreases as throttling is increased to the surge limit. Imposing a physically incorrect stall cell width (for the flow conditions) by fixing the periodicity is shown to result in an instability in the computations. The slope of the phase plot keeps changing with time, and there is a sensitive dependence on the initial conditions and the nonphysical parameters such as the time step and the number of vortices. As already remarked, the vortex method has a random content and thus

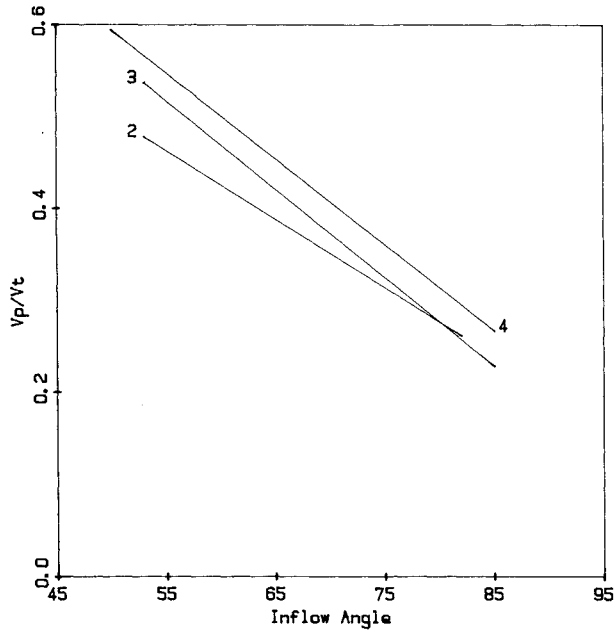

Fig. 12 Influence of the stall-cell wavelength on the stall propagation velocities for 0-deg stagger cascades.

never reproduces exactly the same results for even small changes in parameters. It was found that in some regions of the parameter space, a small change in nonphysical parameter (say 1% change in time step) results in a small (but random) change in the velocity of propagation, whereas in other regions, the same small change results in a large change in the velocity. This was used as an operational definition of stability, and the stability margins were individually established for each flow variable before curve fitting the data.

Figures 10 demonstrate this for a specific case. In Figs. 10a and 10b, the phase plots for a two-blade cascade with a 10-deg stagger, subject to an oncoming flow at 76 deg are shown for two different time steps. The slope clearly does not change significantly for these two cases. On the other hand, as can be seen from Figs. 10c and 10d for the same two-blade, cascade, 63-deg inflow angle, the same small change in the time step generates a large change in the slope of the phase plot.

Figure 11 shows the raw data that form the basis for the computational results of Fig. 9. These data are for a two-blade cascade set at zero stagger. The data are plotted as the period of propagation, which is defined as the time taken for the stall to cross one spatial period vs the inflow angle. There is a band of tightly clustered points from 53 to 70 deg and a region extending up to 82 deg where the points are not as tightly clustered but still close enough to show the trend. Outside these limits, the points are wide apart indicating that there is no stable propagating stall.

A summary of the influence of wavelength on stall propagation is presented in Fig. 12 for a cascade with zero stagger. As can be seen, the stable region of stall propagation extends from 55 to 85 deg for cascades with two-, three-, and four-blade passages with the stall propagation velocity decreasing linearly with increasing inflow angle. The reason for the large incidence angles needed for stable propagating stall is the inadequacy of the boundary-layer model, which predicts attached flow for smaller angles. Within the stable ranges as determined by the above process, the results are consistent and independent of the time step, the number of vortices, the number of boundary points, and other arbitrary parameters in the algorithm such as the vortex core size and the vortex sheet offset distance from the blade surface.

The above discussion of the stability considerations and the ability of a real compressor to pick its own stall wavelength

might suggest that imposing a stall wavelength a priori must result in incorrect results most of the time. However, this does not necessarily follow. For an isolated rotor with a very high hub/tip ratio and a large number of blades, there might indeed be a physically unique stall-cell wavelength corresponding to each set of inflow conditions. In reality, however, compressors typically have many stages and have moderate hub/tip ratios. It has been observed in numerous instances[5,11,12] that in multistage compressors, the stall extends axially through the compressor. In other words, the same stall wavelength exists in all the stages in spite of the vastly different flow conditions. Even in the present experimental work, it was established conclusively that the stall cell extends axially through the rotor in spite of large radial variations in flow conditions due to IGV twist, radially varying wheel speed, and geometrical differences (e.g., in solidity). The conclusion is that except for one "stall instigating section," the rest of the rotor and the rest of the stages of any physical compressor undergoing rotating stall are always operating under an "imposed" stall wavelength. Thus, it is of great interest to know the response of a cascade to imposed wavelengths. If the propagating stall with a certain wavelength is unstable in a particular cascade, it might prevent the entire compressor from entering that mode. The basic problem with the present simulation is not that the stall wavelength is specified in advance but that due to computer limitations, only a certain number of integral number of blade pitches can be used. This may be corrected in the future by employing more efficient representations. Beyond that, it is necessary to investigate how the one common wavelength is selected. This is another aspect of stability and its prediction that needs to be addressed.

The most serious assumption from the point of view of applicability of the results to physical compressors is the neglect of three-dimensional effects. There are no curvature effects like centrifugal force fields or Coriolis accelerations, and there is no radial flow or pressure gradient allowed. Such conditions may be realistic only in very high hub/tip ratio compressors with a large number of stall cells so that curvature effects can be neglected over the extent of each cell. In addition, the rotor-tip effects are not taken into account. The other major assumption is the neglect of viscosity in the flowfield away from the blade surfaces, but since the principle effect of viscosity, i.e., the boundary-layer separation and vortex shedding, has been incorporated, this is not expected to impose a serious limitation.

One final deficiency in the computational model may be noted. The boundary-layer routine for predicting the time history of the separation points is based on a correlation of separation criteria for static boundary layers. This explains the rather large incidence angles noted previously in the prediction, which correspond to the deep stall condition. An improved boundary-layer routine formulation is needed for quantitative predictions.

From an experimental point of view, the frequency of the stall propagation can be determined with considerable precision using the hot-wire anemometer and a spectrum analyzer. For comparison with the computational results, however, the normalized velocity of propagation and the inflow velocity angle need to be known accurately. This determination of the flow speeds and directions has the most uncertainty associated with it, mainly due to problems inherent in hot-wire anemometry itself.

The low hub/tip (0.6) ratio of the experimental compressor poses some problems in the interpretation of the results. The flow angles and the geometrical parameters, like solidity, all vary significantly along the blade height. It is not known which is the stall initiating section or even if the same section is the initiating section at all conditions. For the purposes of comparison, the measured stall propagation was assumed to have been initiated at the mean radius.

VI. Conclusions

The following conclusions may be drawn from the results of the computational and experimental work and their comparisons. Within the regions of stable-stall propagation, the discrete vortex method gives consistent and reproducible results for the quantities of interest. These results are independent, within the wide limits, of the various program-related parameters such as the time step and the vortex core size.

Rotating stall has been shown to have a complex dependence on many parameters, such as the relative inflow angle, the cascade stagger, and the stall width. Computed stall propagation velocity decreased with inflow angle at low stagger angles but increased at high stagger angles. It also increased with the blade solidity and stall-cell wavelength. The effect of blade camber was found to be primarily on the stall inception point, and there is little effect on the propagation velocity.

It was shown experimentally that in one particular compressor, the Stevens axial compressor test rig, the stall cell extends radially through the flow annulus, with the stall intensity highest at the tip. Detailed flow velocity measurements were made during the passage of the stall. Normalized propagation velocity was found to increase with the relative inflow angle and to decrease with the flow coefficient in agreement with the computed results and previous experimental data. The actual values of the velocity propagation were higher than those obtained from computation correlating with the larger stall-cell wavelength in the experiment.

In summary, it has been demonstrated effectively that the two-dimensional treatment results in a prediction that is qualitatively descriptive of the propagating stall phenomenon. The results should be useful, and quantitively correct, for higher hub/tip ratios. The most important applications, however, are those in which the front stages of a compressor are involved. Here the blades are usually of higher aspect ratio, that is, more flexible, and where the lower hub/tip ratios mandate a three-dimensional formulation of the computational algorithm. These refinements, including larger imposed wavelengths and better boundary-layer description, should become increasingly feasible to analyze as supercomputer capacity and speed continue to increase.

Acknowledgments

This work was supported by the Office of Naval Research under Contracts N00014-86-K-0315 and N62271-87-M-0204 for which R. P. Shreeve of the Naval Postgraduate School served as the Project Monitor. P. R. Spalart provided a computer code that served as the starting point of this investigation, and P. Kutler made time available on the Cray X-MP/48 supercomputer at the NASA Ames Research Center. Acknowledgment is also made to the Stevens Institute of Technology for the use of the Institute's computer system.

References

[1]Stetson, H. R., "Designing for Stability in Advanced Turbine Engines," AGARD Rept. CP-3424, 1982.

[2]Yershov, V. N., "Unsteady Conditions of Turbodynamics Rotating Stall," U.S. Foreign Technology Division Translation Paper FTD-MT-24-04-71, 1971.

[3]Stenning, A. H., "Rotating Stall and Surge," *ASME Journal of Fluids Engineering*, Vol. 102, March 1980, pp. 14 20.

[4]Kriebel, A. R., Seidel, B. S., and Schwind, R. G., "Stall Propagation in a Cascade of Airfoils," NACA Technical Memorandum TN 4134, 1958.

[5]Day, I. J., and Cumptsy, N. A., "The Measurement and Interpretation of Flow within Rotating Stall Cells in Axial Compressors," *Journal of Mechanical Engineering Science*, Vol. 20, April 1978, pp. 101 115.

[6]Spalart, P. R., "Two Recent Extensions of the Vortex Method," AIAA Paper 84-0343, Jan. 1984.

[7]Jonnavithula, S., "Computational and Experimental Investigations of Rotating Stall in Compressor Cascades," Ph.D. Thesis, Dept. of Mechanical Engineering, Stevens Institute of Technology, Hoboken, NJ, 1988.

[8]Lamb, H., *Hydrodynamics*, Dover, 1945.

[9]Sisto, F., Jonnavithula, S., and Thangam, S., "Computational Study of the Effect of Cascade Parameters on Stall Propagation in Axial Compressors," *Proceedings of the Symposium on Advances and Applications in Computational Fluid Dynamics*, Vol. 66, edited by O. Baysal, Vol. 66, ASME/FED, 1988, pp. 101–107.

[10]Speziale, C. G., Sisto, F., and Jonnavithula, S., "Vortex Simulation of Propagating Stall in a Linear Cascade of Airfoils," *ASME Journal of Fluids Engineering*, Vol. 108, Sept. 1986, pp. 304–312.

[11]Das, D. K., and Ozcanli, S. C., "An Experimental Study of the Unsteady Response of the Rotor Blades of an Axial Flow Compressor Operating in the Rotating Stall Regime," AIAA Paper 83-0001, Jan. 1983.

[12]Moore, F. K., "A Theory of Rotating Stall of Multistage Axial Compressors, Parts 1–3," *ASME Journal of Engineering for Gas Turbines and Power*, Vol. 106, April 1984, pp. 313–336.